Active Flutter Suppression for Two-Dimensional Airfoils

H. Ohta* and A. Fujimori†
Nagoya University, Furo-cho, Chikusa-ku, Nagoya, Japan
and
P. N. Nikiforuk‡ and M. M. Gupta‡
University of Saskatchewan, Saskatoon, Saskatchewan, Canada

Active flutter suppression for a two-dimensional typical airfoil in an incompressible flow is studied in this paper. The root loci of the systems described by three aerodynamical models, each with a single feedback variable, are first investigated to obtain a physical understanding of these systems. Practical systems that include actuator and gust models are considered next, using linear-quadratic regulator theory. Reduced-order models are constructed using a sequence of truncations based on the modal cost analysis, and modal truncation is examined for several weightings of the cost function. The resulting increases in the performance index and the closed-loop poles are then calculated for each truncation. The essential feedback modes and their associated gains for flutter suppression are determined using this analysis. For a reasonable degree of control, these reduced-order models are sufficiently robust.

Nomenclature

a = nondimensional distance from semichord to the elastic axis.
b = semichord length
$C(\bar{s})$ = generalized Theodorsen function
c = nondimensional distance from semichord to the trailing-edge flap hinge line
$\boldsymbol{F}_a$ = aerodynamic load vector
$\boldsymbol{F}_g$ = gust load vector
h = bending displacement
I = unit matrix
i = $\sqrt{-1}$
J = performance index
K = U/b, a scaled velocity
K_α, K_z = torsional and bending gains, respectively
k = $b\omega/U$, reduced frequency
M = transform matrix
Q, R = weighting matrices
$\boldsymbol{T}_b$ = input torque vector
s = Laplace transform
$\bar{s}$ = sb/U, nondimensional Laplace transform variable
U = freestream velocity
$\boldsymbol{u}$ = input vector
w_g = state of gust model
$\boldsymbol{x}$ = n-state vector of the modal coordinate
$\boldsymbol{x}_p$ = n-state vector of the controlled plant
$\boldsymbol{x}_r$ = n_r-state vector of the reduced-order model
$\boldsymbol{x}_t$ = $(n - n_r)$-state vector of the truncated model
x_α = nondimensional static moment of wing section per unit length about elastic axis
x_β = nondimensional static moment of trailing-edge flap about hinge
$\boldsymbol{y}$ = m-output vector
z = h/b, nondimensional bending displacement
$\boldsymbol{z}_a$ = augmented state vector for $C(\bar{s})$
$\boldsymbol{z}_g$ = augmented state vector for $\psi(\bar{s})$
α = torsion angle of wing, nose upward is positive
β = trailing-edge flap angle, tail downward is positive
β_i = trailing-edge flap command input
γ_α^2 = nondimensional moment of inertia of wing section per unit length
γ_β^2 = nondimensional moment of inertia of trailing-edge flap
$\psi(\bar{s})$ = Küssner function
μ = nondimensional mass
$\omega_h, \omega_\alpha, \omega_\beta$ = natural frequencies of bending, torsion, and flap modes, respectively
ρ = atmospheric density

Introduction

FUTURE energy-efficient transports and control-configured vehicles may require active control technologies (ACT) to realize the full benefits of proposed improvements to their aerodynamics and energy systems. Active flutter suppression (AFS) is one such ACT concept, and its aim is to increase the critical flutter velocity by activating the control surfaces according to the bending and torsion of the wing. The complete dynamics describing such aeroelastic systems, however, are described by partial differential equations for both structural and aerodynamic modeling, and the state-space equations required for the design of a controller may thus require a large number of states to represent such dynamics accurately. As well, an optimal control law based on the standard linear-quadratic Gaussian (LQG) technique would be of the same high order as the plant. Moreover, such a controller would be sensitive to modeling errors and often would be too complex to implement on a flight computer.

To bypass these disadvantages, Mahesh et al.,[1] proposed an LQG synthesis methodology that provides an improved rms response and robust stability. The optimization of the control surface and sensor location were also considered. A method of synthesizing reduced-order optimal control laws was developed by Mukhopadhyay et al.,[2] who employed a nonlinear programming algorithm and proposed a procedure for calculating the feedback gains of some key states. On the other hand, Nissim[3] developed a synthesis methodology using the concept of aerodynamic energy. This technique makes use of the energy required to sustain the simple harmonic oscillations of a two-dimensional typical section of a wing. Several questions concerning the utility of the energy method are discussed in Ref. 4.

Received Aug. 15, 1984; presented as Paper 84-1931 at the AIAA Guidance and Control Conference, Seattle, WA, Aug. 20–22, 1984; revision received Jan. 4, 1988.

*Assistant Professor, Department of Aeronautical Engineering. Member AIAA.
†Graduate student.
‡Professor, College of Engineering.

In spite of the analysis and design that have been carried out in this area, and which have been discussed briefly in the preceding paragraphs, a better insight into the mechanism of flutter is still required to obtain a basic understanding of the order reduction for such aeroelastic models and state feedback control laws. As a contribution to this objective, several AFS systems are discussed in this paper for a two-dimensional typical section of a wing in an incompressible flow.

The behavior of the root loci that leads to aeroelastic instability is first investigated together with the stabilizing effects of the bending and torsional displacement feedback on the system. This study is related to the works of Refs. 4 and 5 using the steady aerodynamic model. However, the characteristics of three aerodynamic models, using steady, quasisteady, and unsteady aerodynamics are illustrated as well. Finally, the modal cost analysis (MCA) introduced by Skelton and Hughes[6] is used to reduce the order of the AFS systems whose design includes both actuator and gust models. The sequence of truncation, the resulting increases of the performance cost, and the closed-loop poles are examined for each truncation. In the process of reducing the order of the AFS systems, the stability region and the response of the control surfaces are discussed and the robustness of the reduced-order AFS system is also investigated.

Description of the Controlled Plant

Consider a two-dimensional typical wing section lying in a uniform freestream velocity U as shown in Fig. 1. The degrees of freedom are the bending displacement h, torsion angle α, and flap angle β of the trailing-edge control surface. The equations of motion are

$$M_s\ddot{\boldsymbol{q}} + D_s\dot{\boldsymbol{q}} + K_s\boldsymbol{q} = \boldsymbol{F}_a + \boldsymbol{F}_g + \boldsymbol{T}_b \tag{1}$$

where $\boldsymbol{q} = [z\ \alpha\ \beta]^T$, the nondimensional bending displacement $z = h/b$, and M_s, D_s, and K_s are, respectively, the generalized mass, structural damping, and stiffness matrices. The structural damping matrix D_s is neglected in the following analysis for the purpose of simplicity.

The aerodynamic load vectors $\boldsymbol{F}_a$ and $\boldsymbol{F}_g$ in Eq. (1) for two-dimensional incompressible flow are given in the Laplace transform with argument s

$$\boldsymbol{F}_a(s) = \rho b^4[KC(ik)RQ_c(s) + Q_{nc}(s)] \tag{2}$$

$$\boldsymbol{F}_g(s) = \rho b^4 KR\psi(ik)w_g \tag{3}$$

where the initial conditions are assumed to be $\boldsymbol{q} = \dot{\boldsymbol{q}} = \boldsymbol{0}$ at $t = 0$. The circulatory load $Q_c(s)$ and noncirculatory load $Q_{nc}(s)$ are described according to the work of Edwards et al.,[7] as

$$Q_c(s) = [E_2 s + KE_1]\boldsymbol{q}(s) \tag{4}$$

$$Q_{nc}(s) = [M_{nc}s^2 + KG_{nc}s + K^2K_{nc}]\boldsymbol{q}(s) \tag{5}$$

where the matrices R, E_1, E_2, and so forth, are described in Ref. 8.

The traditional derivation of the Theodorsen function $C(ik)$ has been assumed to be valid only for simple harmonic motions of the airfoil. This limitation should be removed because subcritical responses of the airfoil are to be examined in the AFS analysis. W. P. Jones concluded that $C(ik)$ could be generalized for diverging airfoil motions, but not for damped converging motions. Still, on the basis of Sears' work on the derivations of the indicial loading functions and using analytic continuation, Edwards has shown that the function $C(\bar{s})$, where $\bar{s} = sb/U$, could be evaluated for an arbitrary value of $\bar{s}$. This function is termed the generalized Theodorsen function.

Noting this generalization, the rational fraction approximation of $C(\bar{s})$ derived by R. T. Jones and the Küssner function

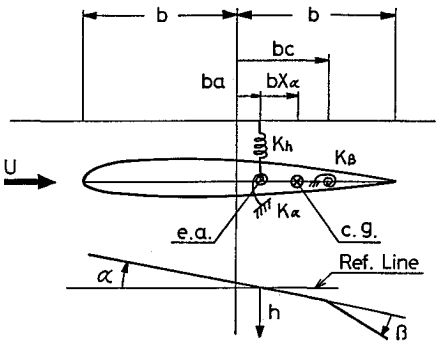

Fig. 1 Two-dimensional airfoil.

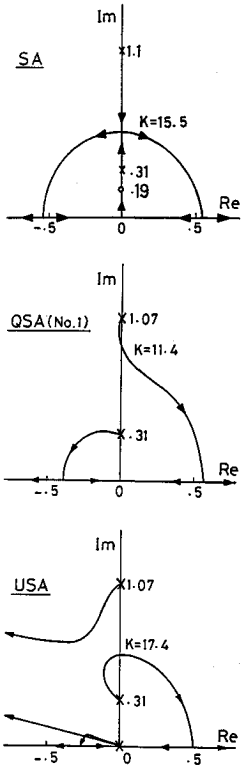

Fig. 2 Root loci for the open-loop system ($K_\alpha = K_z = 0$). Values of K show velocity at which the locus splits from imaginary axis, i.e., the flutter velocity.

$\psi(\bar{s})$ is used to obtain an expression suitable for the design of the controllers.

$$C(\bar{s}) = \frac{0.5\bar{s}^2 + 0.2808\bar{s} + 0.01365}{\bar{s}^2 + 0.3455\bar{s} + 0.01365} \tag{6}$$

$$\psi(\bar{s}) = \frac{0.56\bar{s} + 0.13}{\bar{s}^2 + 1.13\bar{s} + 0.13} \tag{7}$$

With the aid of the augmented state variables z_a and $z_g \in R^2$, the dynamical models of $C(\bar{s})$ in Eq. (6) and $\psi(\bar{s})$ in Eq. (7) may be written as

$$\dot{z}_a = A_a z_a + B_a Q_c \tag{8}$$

$$\dot{z}_g = A_g z_g + B_g w_g \tag{9}$$

where the matrices A_a and B_a are

$$A_a = \begin{bmatrix} 0 & 1 \\ -0.01365K^2 & -0.3455K \end{bmatrix}, \qquad B_a = \begin{bmatrix} 0 \\ 1 \end{bmatrix}$$

and the matrices A_g and B_g can be described in the same way.

The dynamics of the actuator are assumed to be of second order with the controlled angle β_i and the input signal u

$$\ddot{\beta}_i + 2\zeta\omega_n\dot{\beta}_i + \omega_n^2\beta_i = \omega_n^2 u + w_1 \tag{10}$$

where ζ is the damping ratio, ω_n the natural frequency of the actuator, and w_1 denotes a zero-mean white noise disturbance with intensity $4\zeta\omega_n^3\sigma^2$, where σ^2 is the variance of the control surface angle error due to disturbance.

The gust model is assumed to be a first-order system with a white noise input w_2, i.e.,

$$\dot{w}_g = -\omega_g w_g + w_2 \tag{11}$$

where the intensity of w_2 is $2\omega_g\sigma_g^2$ and σ_g^2 is the variance of the gust velocity w_g.

Considering the actuator torque around the flap hinge and its reaction torque around the elastic axis, the input torque T_b becomes

$$T_b = B_0[\beta_i\ \dot{\beta}_i]^T + B_u u \tag{12}$$

Substituting Eqs. (2–12) into Eq. (1), the state equation of the AFS system can be represented by

$$\dot{x}_p = Ax_p + Bu + B_n w \tag{13}$$

where

$$x_p = [q\ \dot{q}\ z_a\ z_g\ \beta_i\ \dot{\beta}_i\ w_g]^T \tag{14a}$$

$$w = [w_1\ w_2]^T \tag{14b}$$

Root Locus Analysis

The dynamical equations required for the root locus analysis of the AFS system are, after letting $F_g = \mathbf{0}$ and $T_b = [0\ 0\ \gamma_\beta^2\omega_\beta^2\beta]^T$ in Eq. (1),

$$\pi[M'_s s^2 + K'_s]q(s) = KC(\bar{s})R'[E_2 s + KE_1]q(s) + [M'_{nc}s^2 + KG'_{nc}s + K^2K'_{nc}]q(s) \tag{15}$$

where the dynamics of the control surface are neglected for simplicity. This leads to the omission of the third equation of Eq. (1) in the analysis, and the superscript $(\ )'$ denotes this omission. The flap angle β is assumed to be linearly related to α or z:

$$\beta = K_\alpha\alpha, \qquad \beta = K_z z \tag{16}$$

where K_α and K_z are the torsion and bending gains, respectively.

Previous works of this kind include that by Rheinfurth and Swift[5] who classified all the possible pole-zero constellations of the system with a steady aerodynamic (SA) model. This work was extended by Horikawa and Dowell[4] for a typical airfoil configuration, where the stability boundaries were expressed in a closed form for different types of feedback signals. Both of these studies were carried out using aeroelastic systems with an SA model whose characteristic polynomial was a biquadratic of s, which allowed a simplified analysis and concise analytical characterization.

To obtain a better understanding of the mechanism of aeroelastic instability, three aerodynamic models will now be considered.

1) *Unsteady aerodynamics (USA).* In this case $C(\bar{s})$, given by Eq. (6), is used in Eq. (15). The characteristic polynomial then becomes of eighth order.

2) *Strict quasisteady aerodynamics (QSA no. 1).* In this case all of the terms in Eq. (15) are considered, but $C(\bar{s})$ is set equal to unity.

Simple quasisteady aerodynamics (QSA no. 2). Here the first term in the right-hand side of Eq. (15), with $C(\bar{s}) = 1$, and the term proportional to $\dot{\alpha}$ in the moment equation, are retained in Eq. (15). The polynomial is then of fourth order.

3) *Steady aerodynamics (SA).* In this situation only the K^2 terms in the first term of the right-hand side of Eq. (15) are retained. This means that the aerodynamic load is determined by the instantaneous values of h and α. The characteristic polynomial then becomes biquadratic as in Refs. 4 and 5.

From the material appearing in Refs. 4 and 7, the following numerical model was selected for this study:

$$\begin{aligned} &\mu = 20, && a = -0.4, && c = 0.5 \\ &\omega_h = \sqrt{5}, && \omega_\alpha = 5\sqrt{2}, && x_\alpha = 0.2 \\ &x_\beta = 0.0125, && \gamma_\alpha^2 = 0.25, && \gamma_\beta^2 = 0.00625 \end{aligned} \tag{17}$$

Root Loci

All of the calculated root loci shown in Figs. 2–4 are symmetric to the real axis. The loci for the QSA no. 2, which are not shown here, can be found in Ref. 8. The root locus of the open-loop system shown in Fig. 2 illustrates the changes that occur between the three aerodynamic models. In particular, the locus of the SA model is located on the imaginary axis when the scaled velocity K is small. The corresponding locus of the USA model, on the other hand, enters the left half of the s plane due to the aerodynamic damping. The root loci of the QSA and USA models are not symmetric to the imaginary axis because the characteristic polynomials include the K term in the QSA model and the K to K^8 terms in the USA model.

The SA and QSA no. 2 models have the same pole-zero configuration. There are two pairs of conjugate poles, denoted by s_1 and s_2, $|s_1| > |s_2|$, and a pair of conjugate zeros on the imaginary axis. The locus of the USA model has four additional poles introduced by the characteristic roots of Eq. (1), i.e., $s = -0.173 \pm i0.043$ (each multiple root) for $K = 0$. The flutter in the SA model occurs at the coupling of two poles, whereas that in the QSA model occurs when the pole s_1 moves toward the right-half plane of s. However, in the USA model

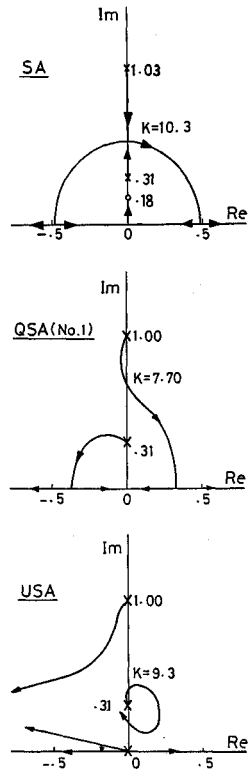

Fig. 3 Root loci for the torsion angle feedback, $K_\alpha = 2.0$.

the pole s can be unstable when positive torsion angle feedback is used, as in Fig. 3c.

Although the locations of the poles change little with variation of the gain K_z of the bending displacement feedback, that of the zero can change significantly. When negative K_z is used, the zero in the SA model is located between the two poles, s_1 and s_2. This means that divergence may occur and no flutter is possible. The converse is true for positive bending feedback if the frequency of the zero is greater than those of the two poles, as shown in Fig. 4a.

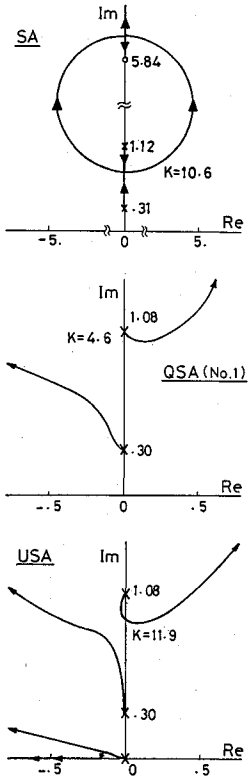

Fig. 4 Root loci for the bending displacement feedback, $K_z = 2.0$.

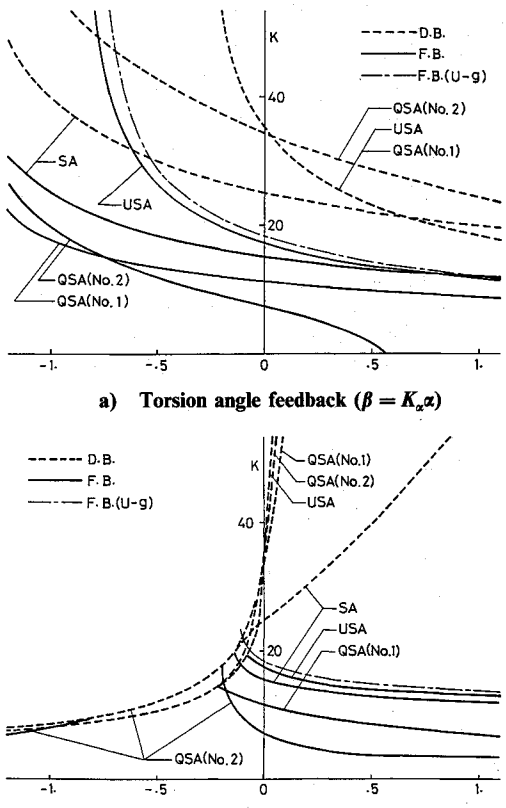

a) Torsion angle feedback ($\beta = K_\alpha \alpha$)

b) Bending displacement feedback ($\beta = K_z z$)

Fig. 5 Stability boundaries.

Stability Regions

Stability regions are shown in Fig. 5 for the three aerodynamic models. The vertical axis is the scaled velocity K, while the abscissa is the feedback gain K_α or K_z. The areas below the flutter boundary lines (F.B.) in this figure represent regions of stability, whereas those above the divergence boundary lines (D.B.) represent regions of instability. The flutter boundary calculated by the U-g method is also illustrated in this figure. As far as divergence is concerned, the QSA no. 1 model predicts the same boundary as the USA model (Fig. 5a). It appears appropriate, therefore, to set $C(\bar{s})$ to unity in the divergence analysis. The QSA no. 2 model for α feedback, on the other hand, does not predict the divergence boundary correctly due to its contracted form.

The flutter boundary of the USA model shows good agreement with that of the U-g method, and the model yields the largest stable region, as shown in Fig. 5a and 5b. It should be noted that the SA model, unlike its contracted form, provides conservative estimates of the flutter boundary with reasonable accuracy. The stability region of the QSA no. 1 model is larger than that of the QSA no. 2 model. This shows that to improve the flutter estimate it is useful to add the effect of the virtual mass to the aerodynamic load.

Flutter onset can be delayed significantly by using negative α feedback (Fig. 5a). As far as z feedback is concerned (Fig. 5b), the positive gain increases the divergence velocity, whereas the divergence, and not the flutter, becomes critical when the negative gains are used. The flutter boundary intersects the divergence boundary at the gain $-0.2 < K_z < -0.1$, which is due to the movement of the zeros. The robustness of the controller requires that care be exercised when gains of approximately these values are used in the design. From the above discussion, it is seen that as far as single feedback is concerned, α feedback is more suitable than z feedback because the region of stability is larger and the controller is less sensitive to the parameter variations. This agrees with the result given in Ref. 4.

Order Reduction of the AFS Systems

The modal cost analysis (MCA) technique, developed by Skelton and Hughes,[6] will be used in this section to eliminate the less significant modes of the optimal closed-loop system derived from the LQ problem. The dynamic equation of the AFS system considered here includes the actuator and the gust models and is given by Eqs. (13) and (14). The outputs of the system are assumed to be the bending displacement z and its acceleration $\ddot{z}$:

$$\boldsymbol{y} = [z \;\; \ddot{z}]^T = C\boldsymbol{x}_p \tag{18}$$

The performance cost for the system is of a quadratic form

$$J = \lim_{T\to\infty} E\left[\frac{1}{T}\int_0^T (\boldsymbol{y}^T Q \boldsymbol{y} + \boldsymbol{u}^T R \boldsymbol{u})\, \mathrm{d}t\right] \tag{19}$$

where R is positive definite and Q is positive semidefinite. The control law that minimizes the performance cost J is given by

$$\boldsymbol{u} = G\boldsymbol{x}_p \tag{20}$$

where G is the optimal feedback gain matrix.

Outline of the Modal Cost Analysis (MCA)

Suppose that the closed-loop matrix $A + BG$ has n distinct eigenvalues. Then, using a coordinate transformation $\boldsymbol{x}_p =$

Mx, $A + BG$ can be transformed to be in the diagonal form

$$M^{-1}(A + BG)M = \Lambda = \text{diag}[\lambda_i], \qquad i = 1,2,...,n \tag{21}$$

Let the vectors c_i and g_i be defined

$$c_i = C\xi_i, \qquad g_i = G\xi_i$$

where ξ_i is the ith column vector of M, i.e., $M = [\xi_1,\xi_2,...,\xi_n]$.

Skelton and Hughes[6] show that when the optimal control law, Eq. (20), is used, the performance cost can be decomposed as

$$J = \sum_{i=1}^{n} J_i = \sum_{i=1}^{n} H_i^* P_i \tag{22}$$

where H_i and P_i represent the ith column vectors of H and P, respectively, and H^* is the complex conjugate transpose of the matrix H. P is defined as

$$P = M^{-1}P_0M^{*-1}, \qquad P_0 = E[x_p(0)x_p(0)^T] \tag{23}$$

and the ijth element of H is given by

$$H_{ij} = \frac{-1}{\lambda_i^* + \lambda_j}(c_i^* Q c_j + g_i^* R g_j) \tag{24}$$

The equation holds if $Re[\lambda_i^* + \lambda_j] < 0$ for all i, j $(=1,...,n)$. Equation (22) shows that the total performance cost J is decomposed to the sum of each modal cost $J_i = H_i^* P_i$. Based on such decomposition, the MCA offers a means for synthesizing a reduced-order controller. That is, those modes that have the largest influence in the cost are chosen to control, and those modes that have the least influence in the cost are truncated. Thus, a reduced controller that is closest in performance to the optimal one can be synthesized.

Among the elements of the modal coordinates x, let the states that are chosen to control be denoted as $x_r \in R^{n_r}$, and let the states that are to be truncated be $x_t \in R^{n-n_r}$. This means that the states x can be decomposed as

$$x = U_r x_r + U_t x_t$$

where $U = [U_r\ U_t]$ denotes a matrix that rearranges the elements of the modal states x according to the significance determined by the MCA. Then, the reduced-order control law is given as

$$u = GMU_r x_r \tag{25}$$

Substituting the control law into Eq. (13), the closed-loop system is given as

$$\begin{bmatrix} \dot{x}_r \\ \dot{x}_t \end{bmatrix} = \begin{bmatrix} \Lambda_r & U_r^T M^{-1}AMU_t \\ 0 & U_t^T M^{-1}AMU_t \end{bmatrix} \begin{bmatrix} x_r \\ x_t \end{bmatrix} + \begin{bmatrix} U_r^T \\ U_t^T \end{bmatrix} M^{-1}B_n w \tag{26}$$

where Λ_r is the diagonal matrix and is equal to $U_r^T M^{-1}(A + BG)MU_r$. Reference 6 offers a method in which a Kalman filter is used to estimate the reduced states x_r. It is assumed in this paper, however, that the states x_r are measurable in order to discuss the basic application of the MCA to the AFS.

The numerical model considered in this MCA is the same as the one given in Ref. 7:

$$\begin{aligned} &\mu = 40, && c = 0.6. && \omega_n = 12\pi \\ &\omega_\alpha = 100, && \omega_h = 50, && \omega_\beta = 300 \\ &\omega_g = 20\pi/3, && \zeta = 0.7 \end{aligned} \tag{27}$$

The other parameters are as given in Eq. (17).

Table 1 Weighting matrices of the performance index

Case	Q[a] q_{11}	q_{22}	R
1	0	0	1
2	1	0	1
3	0	1.E-6	1
4	1	1.E-6	1

[a] $Q = \begin{bmatrix} q_{11} & 0 \\ 0 & q_{22} \end{bmatrix}$

Mode Truncation

The order reduction of the AFS system is examined for selecting the weighting matrices Q and R shown in Table 1. Four cases are considered in this study. Case 1 of Table 1 is the minimum energy solution. This selection implies that the unstable poles are shifted from their unstable position in the

Table 2 Closed-loop poles and truncation sequence (case 3)

Truncation sequence	Mode	Open loop	Closed loop 13 (OPT)	12	11	9	8	7	5	3	2
6	Bending	6.865 $\pm i$70.73	−17.60 $\pm i$31.89	*[a]	*	*	*	*	−16.32 $\pm i$46.10	−8.282 $\pm i$89.25	−2.019 $\pm i$68.33
3	Torsion	−31.42 $\pm i$73.03	−75.28 $\pm i$89.25	*	*	*	*	*	*	*	*
3	Flap	−13.92 $\pm i$340.3	−108.0 $\pm i$362.8	*	*	−10.95 $\pm i$383.1	−9.625 $\pm i$334.1	−15.58 $\pm i$340.8	−13.58 $\pm i$340.5	−13.96 $\pm i$340.3	=
7	Actuator	−26.39 $\pm i$26.92	−33.70 $\pm i$27.63	*	*	*	*	*	*	−28.47 $\pm i$26.06	−26.64 $\pm i$26.65
8	aerod. 1	−80.10	−85.63	*	*	*	*	*	*	*	−78.96
2	aerod. 2	−13.77	=[b]	=	=	=	=	=	=	=	=
5	gust. 1	−325.0	=	=	=	=	=	=	=	=	=
4	gust. 2	−42.25	=	=	=	=	=	=	=	=	=
1	gust. 3	−20.94	=	=	=	=	=	=	=	=	=

[a] * pole is same as optimal closed loop.
[b] = pole is same as open loop.

s-plane to their mirrored position taken with regard to the imaginary axis, but the position of the stable poles remain unchanged. Case 2 is concerned only with the weighting due to the bending displacement, case 3 with the weighting due to the acceleration, and case 4 with the weighting due to both. An optimal regulator was synthesized for each of these cases. The design point was assumed to be at $U/b\omega_\alpha = 3.25$ where the bending mode is unstable and the velocity about 10% higher than at the critical flutter point.

The control gains in the MCA were selected by a sequence of truncations from the optimal gains. This choice was made by comparing the contribution of each mode to the total performance cost. To illustrate how mode truncation was done, an example is shown in Table 2. This is case 3 in Table 1. The aerodynamics 1 and 2 and gusts 1 and 2 denote the modes of z_a in Eq. (8) and z_g in Eq. (9), respectively, and gust 3 denotes the mode of w_g in Eq. (11). Since mode truncation is executed for the closed-loop system, the mode names used in the following correspond to those for the closed-loop system. In Table 2, the gust mode 3 is first truncated to yield a 12th-order system followed, in order, by the truncation of the aerodynamic mode 2 and the flap mode. Although the sequence of mode truncation differed in each case, the gust and flap modes were truncated at an early stage because of the less contribution to the performance cost J.

Since the gust modes 1, 2, and 3 are not controllable, the poles remain unchanged by truncation. It is also to be noted that the truncated modes approached those for the open loop in a stepwise fashion. This is because the mode truncation was done according to the modal cost for the closed-loop modal states. Even though the bending mode that is stabilized in the closed loop may be truncated, the reduced-order AFS system remains stable, and truncation can be continued until the third order is achieved in case 2 and the second order in the other cases. The magnitude of the modal cost is more strongly influenced by the selection of the weighting matrices Q and R than by the eigenvalues of each mode. Consequently, it does not always happen that the modal cost of the closed-loop bending mode makes the largest contribution to the performance cost J. Because the transformation matrix M in Eq. (21) is calculated according to the different reduced-order feedback law at each step, the system matrix in the right side of Eq. (26) is also different for each mode truncation, and some of the truncated modes may become less stable than the corresponding open-loop modes. The flap mode of $n_r = 8$ and 9 in Table 2 shows just the case, although it has still enough stability.

Table 3 shows the increase of the performance index for each mode truncation. The reduced-order system of case 1 is obtained without a deterioration of the index. In cases 2–4, on the other hand, the performance index increases rapidly as the mode truncation proceeds to the third order.

Table 3 Performance index for reduced-order systems

	Case			
Order	1	2	3	4
13	21.9035	174.628	1471.60	1748.04
12	21.9035	174.628	1471.60	1748.04
11	—	—	1471.49	1744.76
10	21.9035	174.623	—	—
9	21.9035	174.624	1471.54	1746.42
8	21.9035	174.636	1523.32	1714.20
7	21.9035	174.630	1508.90	1672.32
6	21.9034	—	—	—
5	—	181.453	1611.18	1955.36
4	21.9034	—	—	—
3	—	213.188	2067.87	2158.28
2	21.9034	—	2977.92	2859.05

Robustness Consideration

Figure 6 shows the Nyquist plots of the optimal and the minimum reduced-order systems for each case. The difference between the full- and reduced-order systems in case 1 is not distinguishable. Although the contours of the Nyquist plot of the reduced-order systems in cases 3 and 4 are smaller than those of the full-order optimal system, the stability margins of the reduced-order systems may be acceptable.

Table 4 shows the stability margins and the rms responses of the flap angle and its velocity. The gain margins and control activities of the minimum reduced-order models deteriorate compared with those of the optimal systems except for case 1. An example of this situation is given in Table 5, which shows the stability margin and rms activities for case 3 for each mode truncation. The deterioration of the gain margin coincides with

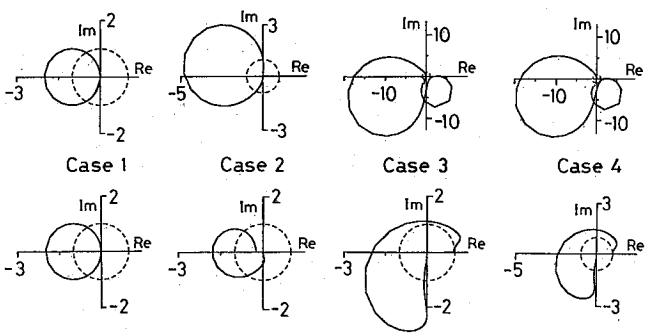

Fig. 6 Nyquist plots. (Upper figures show plots for full-order feedback and lower ones show plots for minimum reduced-order feedback. The radius of dashed circles is unity.)

Table 4 Comparison of stability margins and rms control activities between the full- and reduced-order systems

	Full-order feedback			Reduced-order feedback		
Case	Gain M, dB	Phase M, deg	β_{rms}, deg $\dot{\beta}_{rms}$, deg/s	Gain M, dB	Phase M, deg	β_{rms}, deg $\dot{\beta}_{rms}$, deg
1	−5.905	−60.0	1.748	−5.923	−60.0	1.748
	∞	+60.0	429.7	∞	+59.4	429.7
2	−13.44	−90.0	1.658	−4.947	−48.9	1.901
	∞	+64.5	429.7	∞	+57.0	424.8
3	−24.91	−66.6	1.669	−5.862	−172.2	1.472
	∞	+71.0	129.1	∞	+84.0	415.2
4	−25.33	−72.0	1.511	−7.633	−176.5	1.442
	∞	+70.0	129.0	∞	+82.6	415.6

Table 5 Stability margin for each mode truncation (case 3)

Order	Gain M, dB	Phase M, deg	β_{rms}, deg $\dot{\beta}_{rms}$, deg/s
13	−24.91	−66.6	1.669
	∞	+71.0	129.1
12	−24.93	−67.7	1.686
	∞	+70.9	129.0
11	−24.93	−67.5	1.684
	∞	+70.6	129.0
9	−25.45	−65.5	1.910
	∞	+12.0	408.9
8	−23.02	−51.2	2.223
	+13.59	+76.2	489.2
7	−23.44	−54.6	1.934
	∞	+81.0	382.0
5	−21.93	−95.7	1.598
	∞	+80.5	419.1
3	−15.27	−158.0	1.444
	∞	+81.0	407.5
2	−5.862	−172.2	1.472
	∞	+84.0	415.2

the change in the performance index in Table 3, and increases suddenly for the third order. The control activities, on the other hand, tend to deteriorate near the ninth order. Examination of the other cases shows that the degradation of the performance index leads to the deterioration of the stability margins and the control activities. As a result, the desirable reduced-order systems are of fifth order in case 2 and of third order in cases 3 and 4. In case 1, however, even the second order system is acceptable.

Conclusions

Studies were carried out to obtain a better understanding of two-dimensional active flutter suppression systems. The effects of feedback on the stability and on the characteristics of the airfoil were examined using the root loci technique. It was shown that torsion angle feedback yields a larger stabilized region than bending displacement feedback, and that the airfoil characteristics become less sensitive to parameter variations.

A study of modal truncation was also made using the modal cost analysis procedure. It was found that the optimal system can be truncated as low as third order in the example considered without any significant degradation of the performance. This suggests the application of this method to the control of unsteady three-dimensional wings modeled by the matrix Padé approximation. The design of state estimators based on the reduced-order systems derived here are of practical importance, and will be studied in the future.

Acknowledgment

Part of this research was supported by the Natural Sciences and Engineering Research Council of Canada under Grants A-5625 and A-1080, and part by a Grant-in-Aid Research Project for Scientific Research by the Ministry of Education and Science of Japan.

References

[1]Mahesh, J. K., Stone, C. R., Garrard, W. L., and Dunn, H. J., "Control Law Synthesis for Flutter Suppression Using Linear Quadratic Gaussian Theory," *Journal of Guidance and Control*, Vol. 4, July–Aug. 1981, pp. 415–422.

[2]Mukhopadhyay, V., Newsom, J. R., and Abel, I., "Reduced-Order Optimal Feedback Control Law Synthesis for Flutter Suppression," *Journal of Guidance, Control, and Dynamics*, Vol. 5, July–Aug. 1982, pp. 389–395.

[3]Nissim, E., "Comparative Study Between Two Different Active Flutter Suppression Systems," *Journal of Aircraft*, Vol. 15, Dec. 1978, pp. 843–848.

[4]Horikawa, H. and Dowell, E. H., "An Elementary Explanation of the Flutter Mechanism with Active Feedback Controls," *Journal of Aircraft*, Vol. 16, April 1979, pp. 225–232.

[5]Reinfurth, M. H. and Swift, F. W., "A New Approach to the Explanation of the Flutter Mechanisms," NASA TN-D-3125, Jan. 1966.

[6]Skelton, R. E. and Hughes, P. C., "Modal Cost Analysis for Linear Matrix-Second Order-Systems," *Transactions of the ASME, Journal of Dynamic Systems, Measurement, and Control*, Vol. 102, Sept. 1980, pp. 151–158.

[7]Edwards, J. W., Breakwell, J. V., and Bryson, A. E., Jr., "Active Flutter Control Using Generalized Unsteady Aerodynamic Theory," *Journal of Guidance and Control*, Vol. 1, Jan.–Feb. 1978, pp. 32–40.

[8]Ohta, H., Fujimori, A., Nikiforuk, P. N., and Gupta, M. M., "Control Law Synthesis for Active Flutter Suppression Based on the Modal Cost Analysis," *Proceedings of the AIAA Guidance, Navigation, and Control Conference*, AIAA, New York, 1984, pp. 535–543.

[9]Theodorsen, T. and Garrick, I. E., "Non-Stationary Flow About a Wing-Aileron-Tab Combination Including Aerodynamic Balance," NACA Rept. 736, 1942.